Welding in the World

Regulation of welding residual stress in laser-welded AISI 304 steel- niobium joints using a Cu interlayer

--Manuscript Draft--

Manuscript Number:	WITW-D-21-00167R1
Full Title:	Regulation of welding residual stress in laser-welded AISI 304 steel- niobium joints using a Cu interlayer
Article Type:	Research Paper (unsolicited)
Corresponding Author:	Jingyong Li Jiangsu University of Science and Technology CHINA
Corresponding Author Secondary Information:	
Corresponding Author's Institution:	Jiangsu University of Science and Technology
Corresponding Author's Secondary Institution:	
First Author:	Mingxiao Shi
First Author Secondary Information:	
Order of Authors:	Mingxiao Shi
	Jiugong Chen, M.D
	Jingyong Li
	Weidong Mao
	Shengliang Li
	Xiang Ma
	Huifeng Ni
	Haochun Xia
Order of Authors Secondary Information:	
Funding Information:	national natural science foundation of china (51605205) — Dr. Mingxiao Shi
Abstract:	Residual stress and deformation in a welded joint will significantly reduce its service life, and thus the analysis and regulation of residual stresses are very important. In this paper, a SYSWELD software was used to numerically simulate the temperature field, residual stress field, and the welding deformation during welding with and without a Cu interlayer. Thermocouples were used to measure the thermal cycle curves, and X-ray diffraction (XRD) was used to measure the residual stresses of the joints. The results show that the addition of a Cu interlayer does not significant change the temperature field, and that the high temperature region on the niobium side is wider. In addition, the peak temperature in the centre of the welds and the temperature gradient perpendicular to the weld are greatly reduced by a Cu interlayer. Furthermore, a Cu interlayer contributes to a certain increase in both transverse and longitudinal residual stresses. Because the weld involves three different materials, steel, niobium, and Cu, the residual stresses in the welds are more complex. The simulation of the welding deformation shows that the transverse shrinkage in the thickness direction can be homogenized by the Cu interlayer, which leads to a significant reduction in deformation.

Regulation of welding residual stress in laser-welded AISI 304 steel-niobium joints using a Cu interlayer

Mingxiao Shi[1], Jiugong Chen[1], Jingyong Li[1, *], Weidong Mao[2,3], Shengliang Li[2,3], Xiang Ma[4], Huifeng Ni[5], Haochun Xia[5]

1. School of Materials Science and Engineering, Jiangsu University of Science and Technology, Zhenjiang 212003, China

2. Chery New Energy Automobile Co., Ltd., Wuhu 241003, China

3. Anhui Key Laboratory of New Energy Automobile Lightweight Technology, Wuhu 241003, China

4. Department of Industrial Process Technology, SINTEF Materials and Chemistry, Oslo 0314, Norway

5. Shanghai Jiangnan Shipyard, Shanghai 201913, China

Abstract

Residual stress and deformation in a welded joint will significantly reduce its service life, and thus the analysis and regulation of residual stresses are very important. In this paper, a SYSWELD software was used to numerically simulate the temperature field, residual stress field, and the welding deformation during welding with and without a Cu interlayer. Thermocouples were used to measure the thermal cycle curves, and X-ray diffraction (XRD) was used to measure the residual stresses of the joints. The results show that the addition of a Cu interlayer does not significant change the temperature field, and that the high temperature region on the niobium side is wider. In addition, the peak temperature in the centre of the welds and the temperature gradient perpendicular to the weld are greatly reduced by a Cu interlayer. Furthermore, a Cu interlayer contributes to a certain increase in both transverse and longitudinal residual stresses. Because the weld involves three different materials, steel, niobium, and Cu, the residual stresses in the welds are more complex. The simulation of the welding deformation shows that the transverse shrinkage in the thickness direction can be homogenized by the Cu interlayer, which leads to a significant reduction in deformation.

Key words

AISI304; niobium; temperature field; residual stress; deformation

1 Introduction

With the rapid development of modern processing technology, dissimilar metal welding has become widely used in engineering manufacturing. The welding structure of dissimilar metals can reduce the cost and take full advantage of their respective properties (Refs. 1–3). During the operation of particle accelerators, the superconduct niobium cavities are cooled by liquid helium, which is contained in an austenitic steel vessel (Ref. 4). Thus, its construction inevitably involves the problem of joining niobium to austenitic stainless steel. Similar to most dissimilar metal welding, stainless steel-niobium joints easily form brittle intermetallics (i.e., Fe_2Nb and Fe_7Nb_6), which contribute to brittle failure of the joint (Ref. 5). Explosive welding is the most

commonly used welding method to join steel and niobium, but it is hardly applicable for components with complex shapes (Refs. 6, 7). Welding-brazing and brazing have also been attempted, but an intermetallic layer can form very easily (Ref. 8). Laser welding, an advanced alternative welding method, has the advantages of high energy density, rapid welding speed, and precise control of the heating position. Therefore, it is widely used in welding of dissimilar materials (Ref. 9). Our previous research obtained high-strength AISI 304 steel-niobium laser-welded joints using a Cu interlayer, which has a good metallurgical compatibility with these two base metals (Ref. 10). However, because large residual stresses and deformations exist in the welded joints of dissimilar materials, which could significantly reduce the bearing capacity and service life of the welded joints, the analysis and regulation of residual stresses are very important. K Saito et al. (Ref. 11) used an interlayer to reduce the residual stresses of the joints. The stress fields of P92-SUS 304 dissimilar steel joints welded with interlayers were calculated by numerical methods, and it was found that a suitable interlayer can decrease the residual stresses of the weld. D Travessa et al. (Ref. 12) found that the interlayer has a significant effect on the stresses of the welded joints. When joining Al_2O_3 to AISI 304 steel by diffusion welding, using soft metals Mo and Cu as the interlayer can reduce the residual stresses of the weld. In summary, the addition of a suitable interlayer has a significant impact on the residual stresses and deformations in the joints.

In this paper, based on our previous study (Ref. 10), we added 1.5-mm-thick Cu as the interlayer to join niobium and austenitic stainless steel and used a SYSWELD software to numerically simulate the temperature and stress fields of welding both with and without the Cu interlayer. A comparison of the temperature and stress fields of these two welding methods, shows that the addition of the Cu interlayer can alleviate the temperature gradient and decrease the deformation of the weld, which provides important guidance for the joining of niobium to austenitic stainless steel.

2 Finite element modelling

2.1 Governing equation

The welding temperature field is a nonlinear transient heat transfer process. During the welding process, the governing equation for the analysis of transient heat transfer is:

$$\rho c \frac{\partial T}{\partial t}(x,y,z,t) = -\nabla \cdot q(x,y,z,t) + Q(x,y,z,t),$$

where ρ is the density of the materials (g/mm^2), c is the specific heat capacity ($J/(g\cdot^{\circ}C)$), T is the current temperature ($^{\circ}C$), q is the heat flux vector (W/mm^2), x, y, and z are the coordinates in the reference system (mm), t is the time (s), and ∇ is the spatial gradient operator. The nonlinear isotropic Fourier heat flux constitutive equation is employed:

$$q = -k\nabla T,$$

where k is the temperature-dependent thermal conductivity ($J/(mm \cdot s \cdot ^{\circ}C)$).

During the welding process, a high-energy laser beam acted on a specific path to form a molten pool. The metal gradually solidifies after the heat source is removed. Throughout the process, the state of the material and its thermophysical and mechanical properties change nonlinearly. The results of the calculations were loaded as thermal loads into a thermal-elastic-plastic finite element model for the calculation of welding stresses and deformations. The strain during welding can be described by the following equation:

$$\varepsilon_{total}=\varepsilon_e+\varepsilon_p+\varepsilon_{th}+\varepsilon_{tr}+\varepsilon_c,$$

where ε_e is the elastic strain, ε_p is the plastic strain, ε_{th} and ε_{tr} are, respectively, the thermal strain and solid-state phase transformation strain, and ε_c is the creep strain. Because 304 steel is austenitic stainless steel, the solid-state phase transformation has little effect on the residual stress. Moreover, due to the characteristics of laser welding, the creep phenomenon is not evident, and thus the creep strain can also be ignored.

2.2 Heat source modelling

Due to the concentration of the heat input of the laser beam and the large aspect ratio, a 3D Gaussian heat source was used to characterize the heat flow density distribution of laser welding. The radius of the heat flow distribution in each section decays linearly along the thickness direction. The heat flow density distribution is:

$$q(r,z)=\frac{9Qe^3}{\pi H(e^3-1)(r_e^2+r_e r_i+r_i^2)}\exp(-\frac{3r^2}{r_0^2}),$$

where

$$r_0(z)=r_e-(r_e-r_i)\frac{z_e-z}{z_e-z_i},$$

is the radius of any cross-section of the heat source, r_e and r_i are, respectively, the radii of the upper and lower surfaces of the heat source, z_e and z_i are, respectively, the z-coordinates of the upper and lower surfaces of the heat source, H is the height of the heat source, and Q is the effective laser heat input.

2.3 Mesh division and boundary conditions

Meshing was performed for the steel-niobium direct welding and the laser double-pass welding after the addition of a Cu interlayer. Both the steel and Nb plates were of dimensions 200 mm×200 mm×2 mm, and the Cu interlayer was 200 mm×1.5 mm×2 mm. The mesh near the weld was refined to improve the accuracy of the calculation. The mesh unit at the weld line was a 0.3 mm×0.3 mm×1 mm hexahedron. Fig. 1 shows the mesh model and mechanical boundary conditions. Rigid points were set to limit the translation and rotation of the weldments.

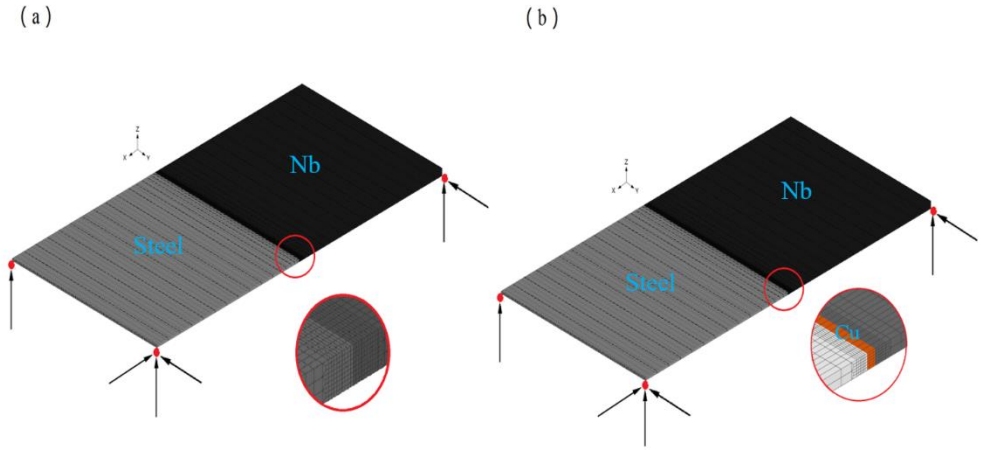

Fig. 1 Mesh model and mechanical boundary conditions for welding (a) without and (b) with a Cu interlayer.

Thermal boundary conditions include the initial conditions of the weldments and the surface heat transfer conditions. The initial temperature condition was set to room temperature, i.e., T_0=20□. Generally, convection heat transfer q_c and radiation heat transfer q_r are considered for the surface heat transfer of weldments. The set of control equations is:

$$\begin{cases} q_c=-h_c(T-T_0) \\ q_r=-\varepsilon\sigma(T^4-T_0^4), \\ q_{loss}=q_c+q_r \end{cases}$$

where q_{loss} is the total heat loss, h_c, the convective heat transfer coefficient, takes a constant value of 30 $W \cdot m^{-2} \cdot ℃^{-1}$, ε is the thermal radiation coefficient, σ is the Stefan-Boltzmann constant, which is $5.67 \cdot 10^{-8}$ $W \cdot m^{-2} \cdot ℃^{-4}$, and T_0 is room temperature.

2.4 Material properties

In this study, three materials were involved: austenitic stainless steel (AISI 304), niobium (Nb), and copper (Cu). The specific parameters required in the numerical simulation are as follows: thermal conductivity, specific heat capacity, density, melting point, elastic modulus, linear expansion coefficient, yield strength, and the Poisson's ratios of the materials. The thermophysical and mechanical properties of the three materials as a function of temperature are shown in Fig. 2.

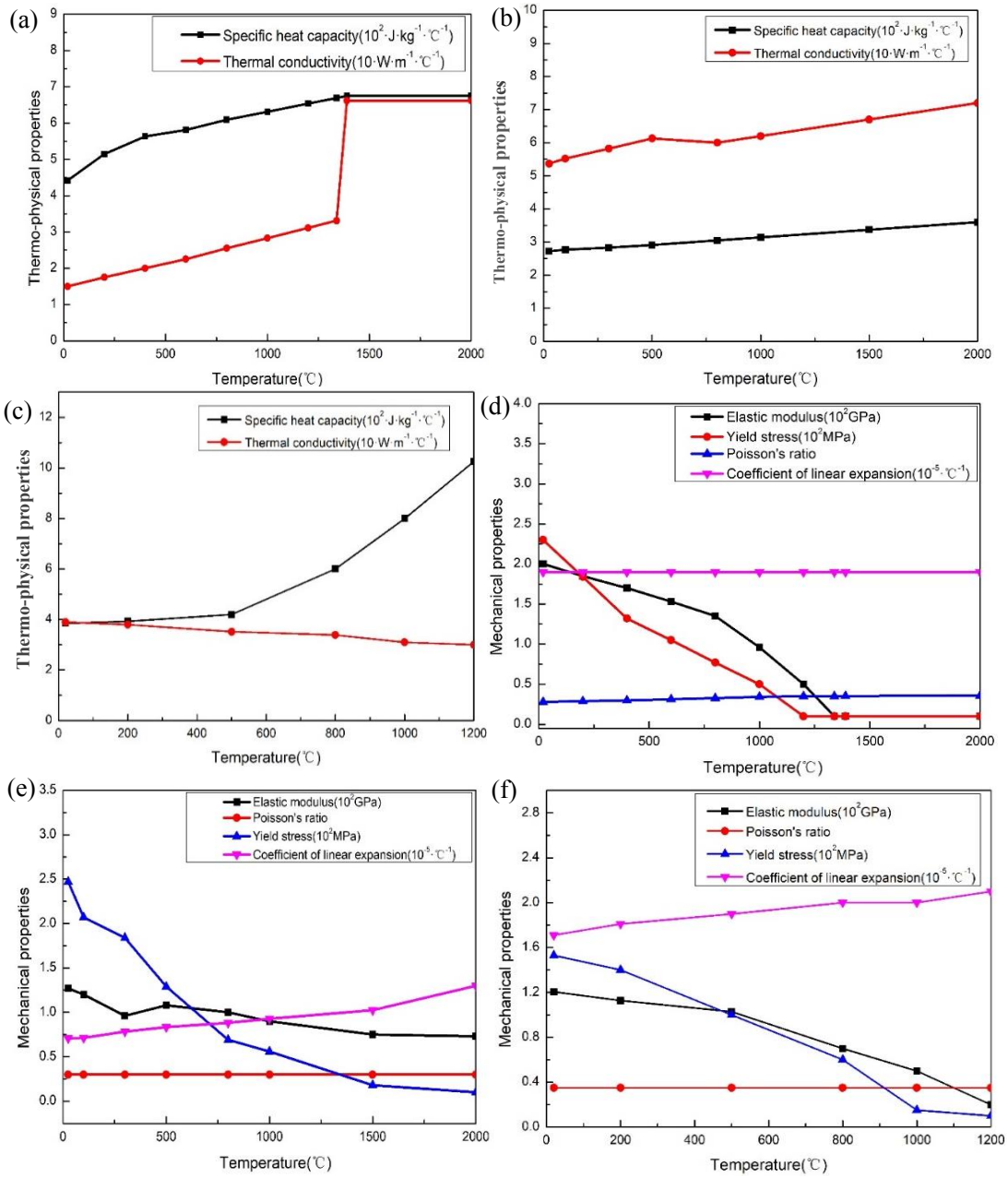

Fig. 2 The thermophysical properties ((a)-(c)) and mechanical properties ((d)-(f)) of AISI 304 steel, Nb, and Cu.

2.5 Measurements of residual stress

The residual stress of the joint was measured by an iXRD-MG40P-FS X-ray diffractometer. Fig. 3 shows the analysis paths of residual stress (RS) and the locations of stress measurements for welding without and with a Cu interlayer.

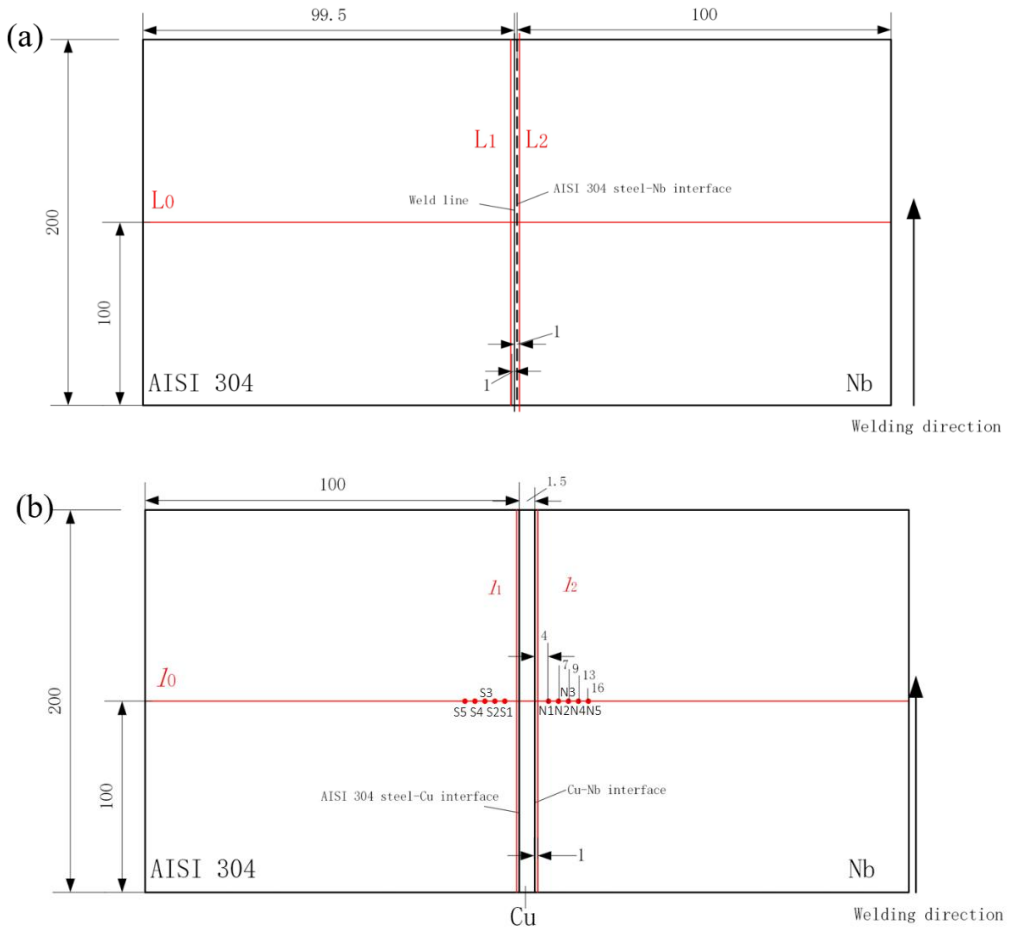

Fig. 3 Schematic diagram of the analysis paths and measurement positions of residual stresses for welded joints (a) without and (b) with a Cu interlayer.

3 Temperature field

Fig. 4 compares the cross-sectional macroscopic appearance of the joint and the simulated molten pools when welding without and with a Cu interlayer. The simulated results are in good accordance with the experimental results.

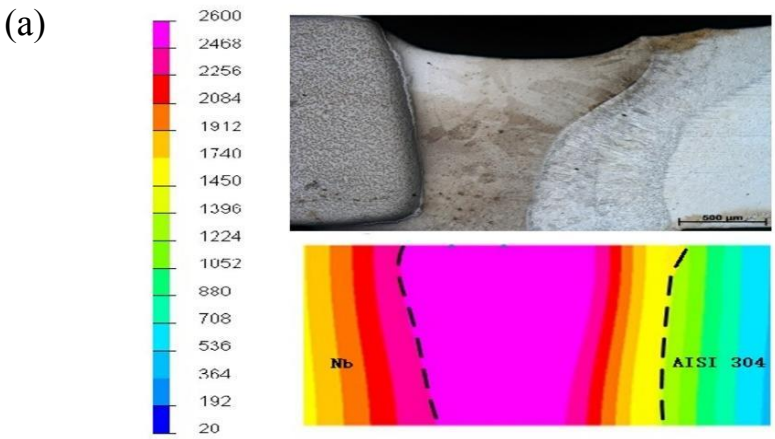

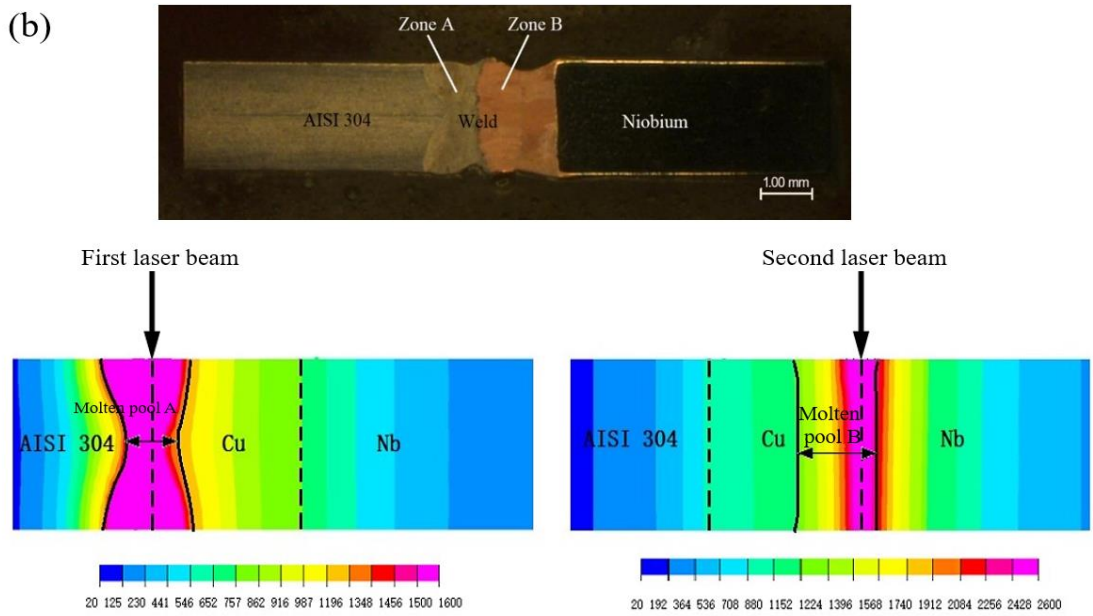

Fig. 4 Comparison between the cross-sectional macroscopic appearance of the joints and the simulated molten pools for welded joints (a) without and (b) with a Cu interlayer.

Fig. 5(a) shows the temperature field at the instant when offset beam welding enters the quasi-steady state. Fig. 5(b) shows the temperature field distribution at the quasi-steady state for the laser double-pass welding with a Cu interlayer. By comparing Fig. 5(a) with Fig. 5(b), we see that the sizes of the molten pool are not significantly different and that their shapes are ellipsoidal. However, the high-temperature regions of the temperature field on the Nb side and the stainless steel side increased after adding a Cu interlayer because the thermal conductivity of Cu is much higher than that of stainless steel and Nb, and it conducts significant heat to the surrounding base materials during welding.

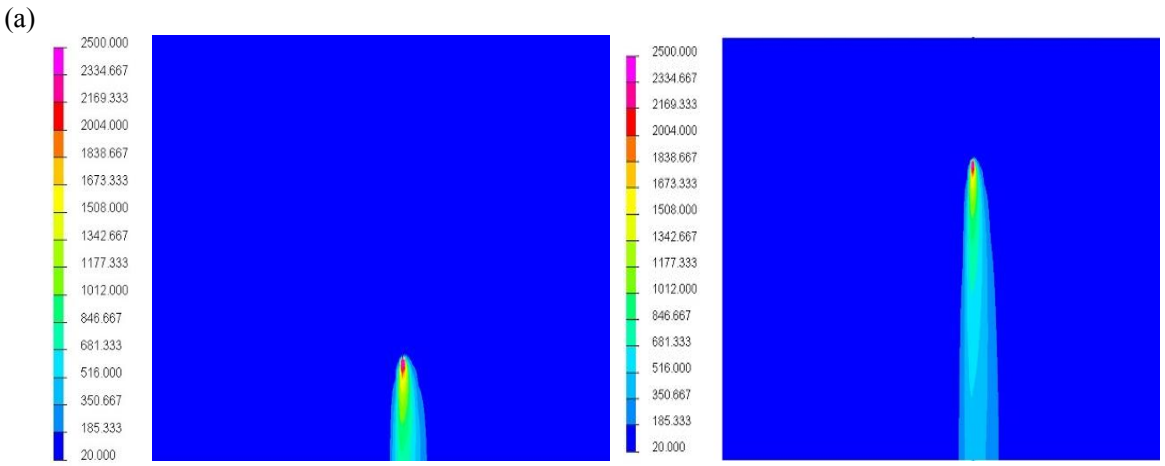

1.7 s

5.7s

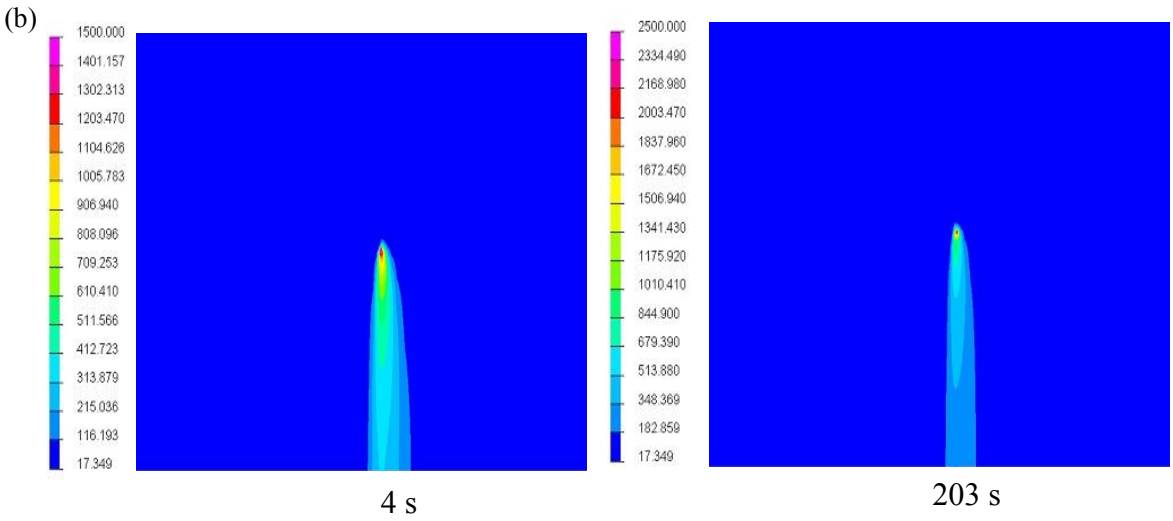

Fig. 5 Cloud diagram of the temperature field at the quasi-steady state instant for welding (a) without and (b) with a Cu interlayer.

For the laser-offset welding, four feature nodes were selected on each side perpendicular to the weld, which were 1, 2, 3, and 4 mm away from the weld. The nodes on the stainless steel side were marked 1, 2, 3, and 4, and those on the Nb side were marked 1', 2', 3', and 4'. Figs. 6(a) and (b) show the thermal cycle curves for the four nodes on the stainless steel side and the Nb side, respectively, when welding without a Cu interlayer. Figs. 6(c) and (d) show the thermal cycle curves of two nodes on the stainless steel side and on the Nb side, respectively, when welding with a Cu interlayer. By comparing Figs. 6(a) and (b) with Figs. 6(c) and (d), we see that the thermal cycle curves of welding with a Cu interlayer are generally similar to those of welding without a Cu interlayer; however, the Cu interlayer results in a lower peak temperature at each node because Cu has high thermal conductivity and causes an increase in heat dissipation. On the stainless steel side, the peak temperature at the characteristic point 1 mm away from the weld centre is approximately 1170℃. When the distance increases to 2 mm, the peak temperature is approximately 250℃, a decrease of nearly 900℃. For welding without a Cu interlayer, the peak temperature drops by approximately 1000℃ at the same positions and distance. Similarly, on the niobium side, the peak temperature decreases by 600℃ when it reaches 2 mm, while the peak temperature of welding without a Cu interlayer decreases by approximately 1000 ℃. The temperature differences between the nodes, which are 1 and 2 mm away on the stainless steel side and the Nb side, are reduced by approximately 100 ℃ and 400 ℃, respectively. The addition of the Cu interlayer can reduce the temperature difference in the vertical direction of the weld and thereby decrease the temperature gradient at the weld. Because the temperature gradient is the main cause of thermal stress, the performance of the joint may be improved by a reduction of the temperature gradient.

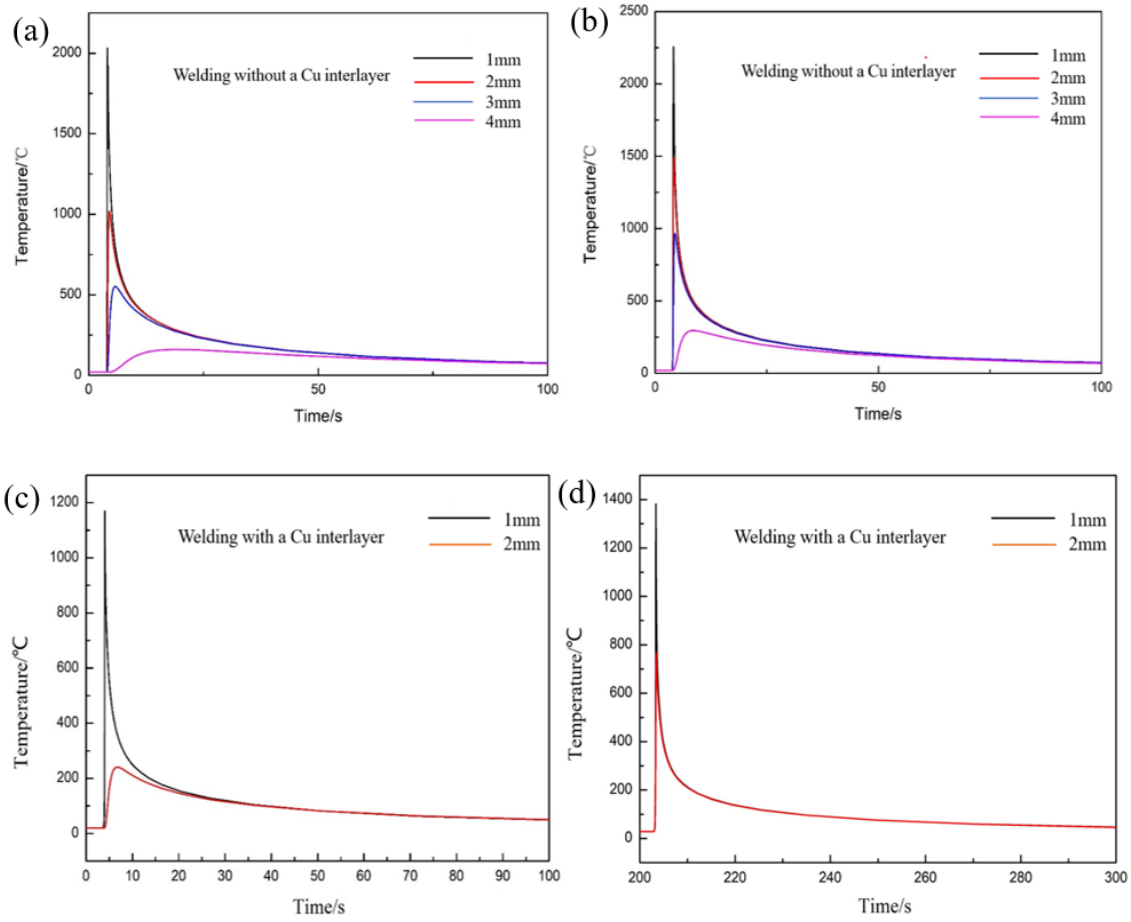

Fig. 6 Thermal cycle curves for nodes on (a) and (c) the stainless steel side and on (b) and (d) the Nb side of the joints.

Fig. 7 shows the thermal cycle curves of the weld centre with and without a Cu interlayer. It can be seen from the figure that the peak temperature of the weld centre decreases by approximately 2000℃ after a Cu interlayer is added because of the high thermal conductivity of Cu.

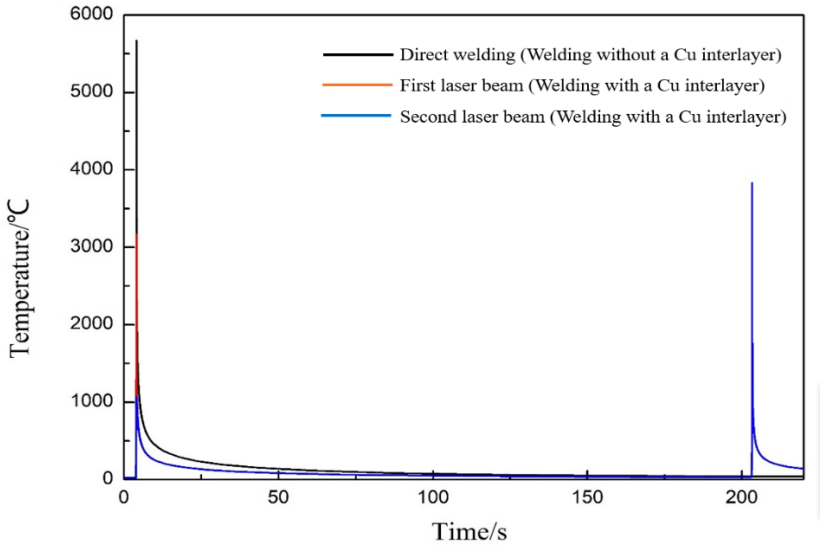

Fig. 7 Thermal cycle curves for the nodes on the centre of the weld.

4 Residual stress field

To verify the accuracy of the numerical simulation when welding with a Cu interlayer, XRD was used to measure the RS of the weld. As shown in Fig. 8, the residual stress distribution curve along l_0 (Fig. 3(b)) is in good agreement with the test points (S1, S2, S3, S4, S5, N1, N2, N3, N4, and N5 in Fig. 3(b)). Discrepancies may be due to the constraining force; for the fixture, these may have changed dynamically during the welding process due to deformation, whereas the numerical simulation used nodes with rigid constraints. In addition, mechanical parameters of the materials during the actual welding process may have differed from the preset values, which can also lead to errors. In general, the maximum error was less than 50 MPa, and thus the accuracy of the simulation can be verified.

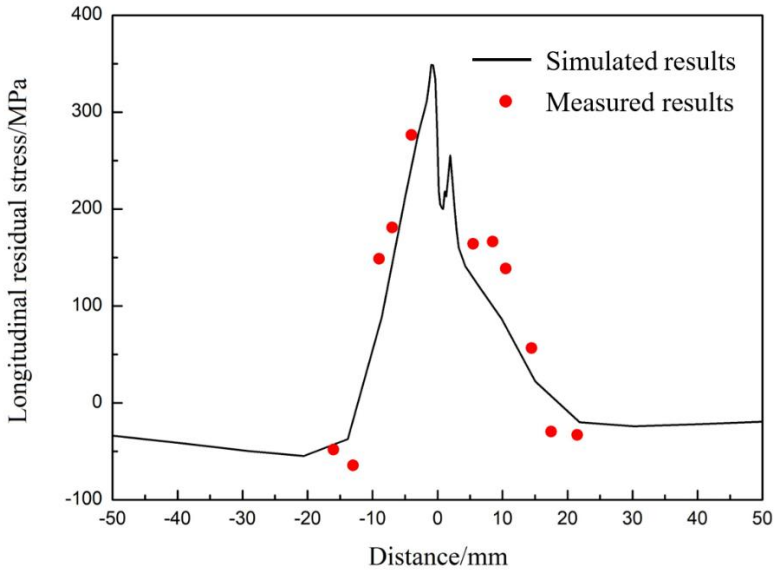

Fig. 8 Thermal cycle curve of the nodes on the centre of the weld for welding with a Cu interlayer.

The longitudinal residual stress (LRS) is the stress parallel to the direction of the weld, represented by σ_y. Fig. 9 shows the longitudinal residual stress distribution with

and without the Cu interlayer. Calculations show that the addition of the Cu interlayer does not significantly change the distribution of the longitudinal residual stress field. Specifically, the weld still exhibits compressive stress, away from the weld area it exhibits tensile stress, and the distribution of residual stress is asymmetrical about the centre of the weld. Fig. 9(b) shows the LRS distribution after the first laser acting on the faying surface of steel and Cu. Fig. 9(c) shows the LRS distribution after the second laser acting. Comparing Fig. 9(a) with Figs. 9(b) and (c), the addition of a Cu interlayer leads to an increase in the LRS. In addition, the LRS is reduced in the middle of the weld because the second laser acted as a heat treatment for the first weld. According to Figs. 9(d) and (e), the addition of a Cu interlayer leads to a more complex LRS distribution in the weld due to the large differences in the mechanical properties of the three materials.

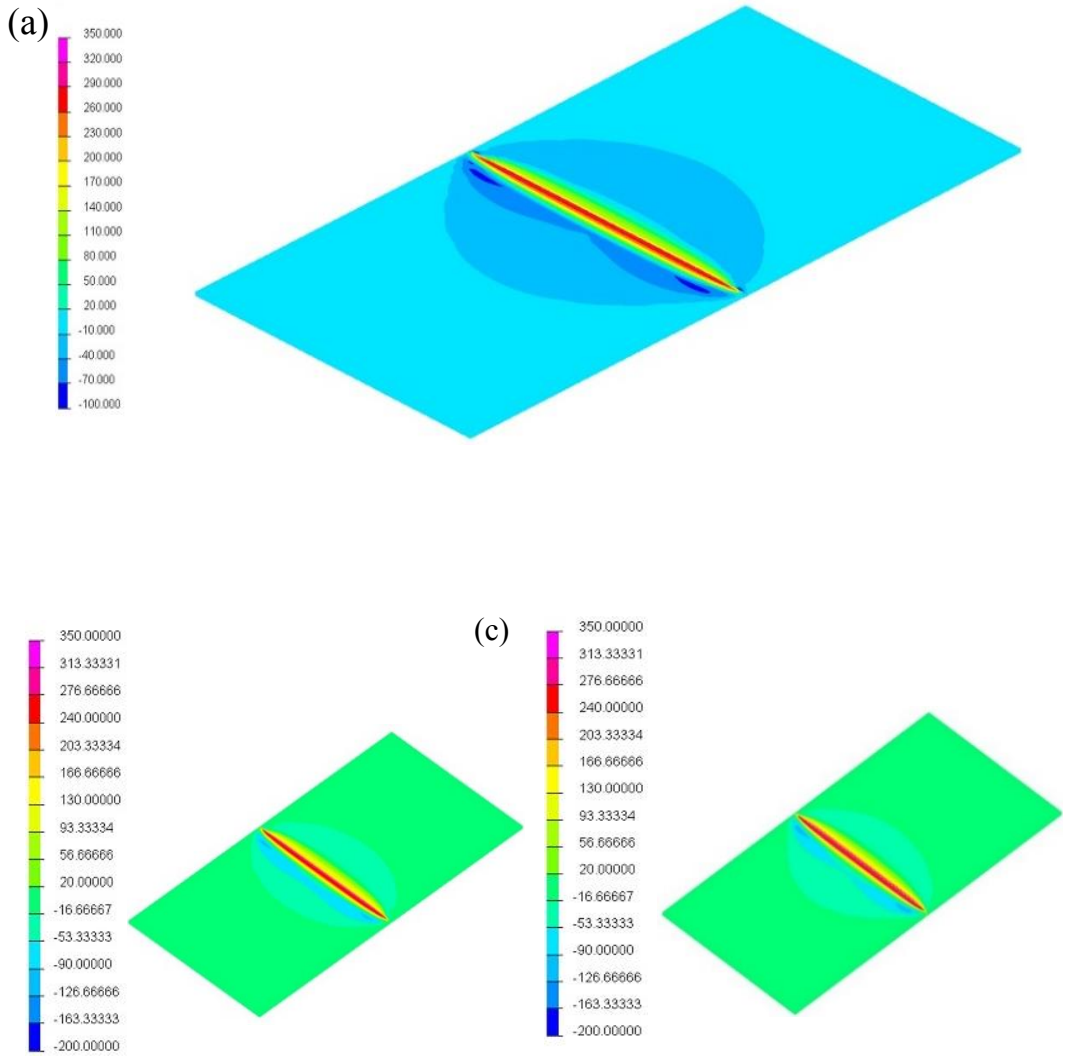

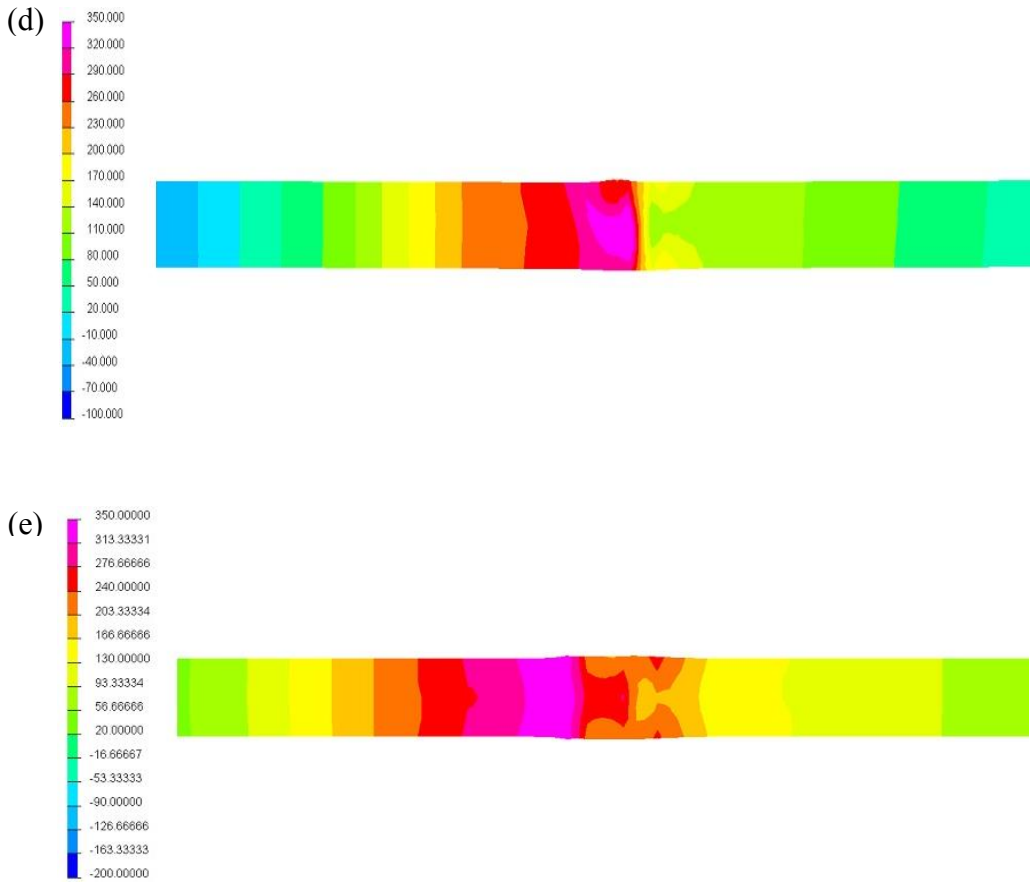

Fig. 9 Longitudinal residual stress distribution for welding (a) without and (b) and (c) with a Cu interlayer. Overall cross-section distribution of longitudinal residual stress for welding (d) without a Cu interlayer and (e) with a Cu interlayer.

The transverse residual stress (TRS) is the RS perpendicular to the weld, represented by σ_x, and is generally considered to be a combination of longitudinal and transverse shrinkage of the weld. Fig. 10 shows the transverse residual stress distribution with and without a Cu interlayer. The calculation results show that the addition of a Cu interlayer results in an imperceptible change in the TRS distribution. Meanwhile, comparing Fig. 10(a) to Figs. 10(b) and (c), the transverse stress becomes larger after the second laser acting, possibly because the two laser heat inputs increase the amount of melted metal and the shrinkage during the cooling process.

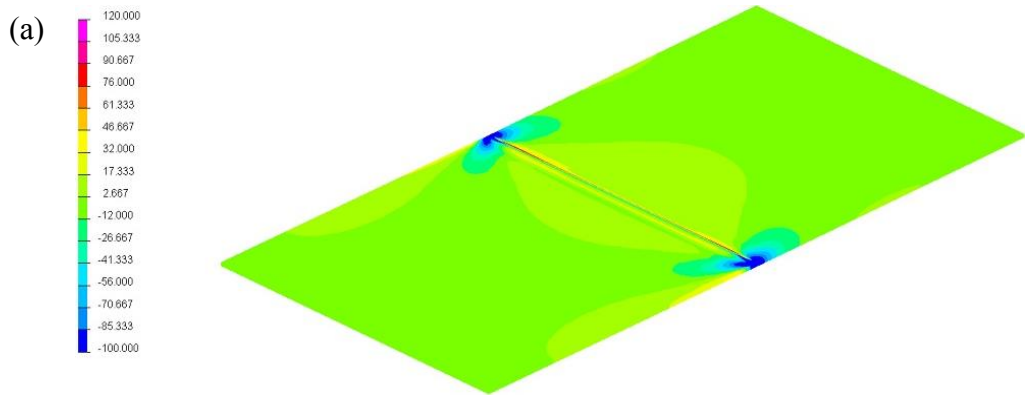
(a)
120.000
105.333
90.667
76.000
61.333
46.667
32.000
17.333
2.667
-12.000
-26.667
-41.333
-56.000
-70.667
-85.333
-100.000

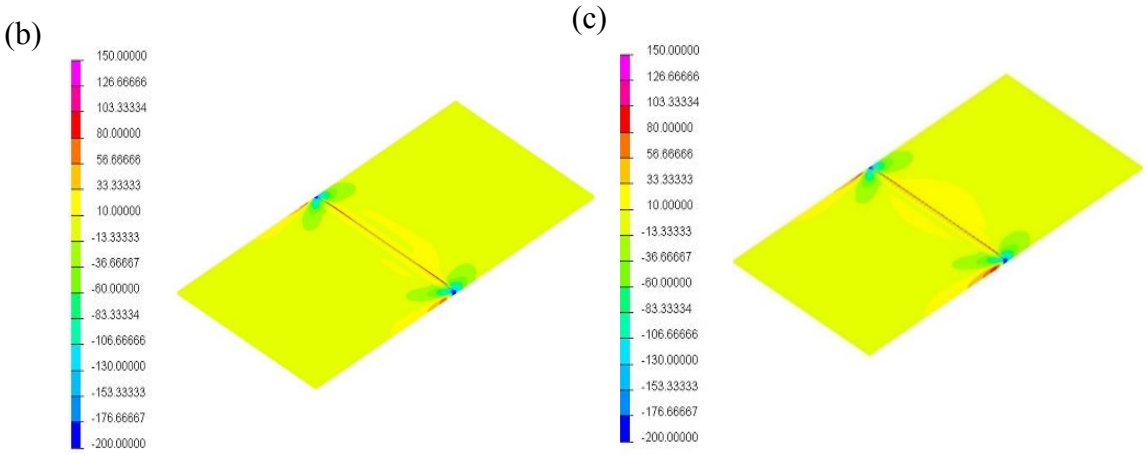
(b)
150.00000
126.66666
103.33334
80.00000
56.66666
33.33333
10.00000
-13.33333
-36.66667
-60.00000
-83.33334
-106.66666
-130.00000
-153.33333
-176.66667
-200.00000
(c)
150.00000
126.66666
103.33334
80.00000
56.66666
33.33333
10.00000
-13.33333
-36.66667
-60.00000
-83.33334
-106.66666
-130.00000
-153.33333
-176.66667
-200.00000

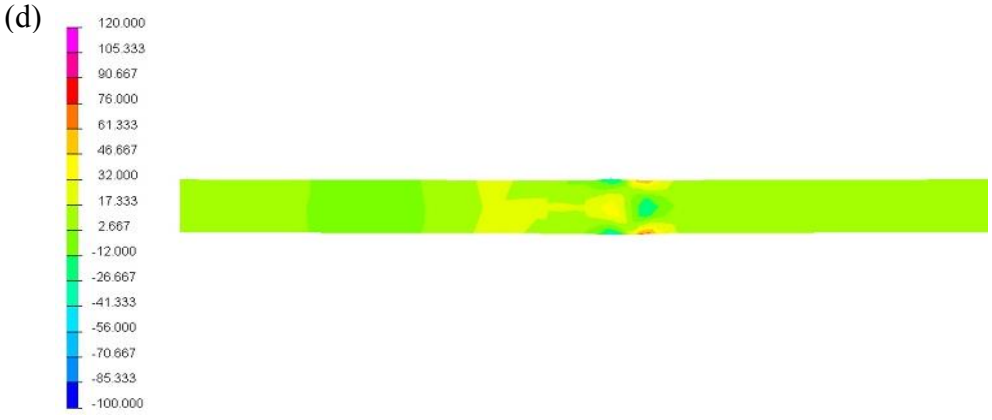
(d)
120.000
105.333
90.667
76.000
61.333
46.667
32.000
17.333
2.667
-12.000
-26.667
-41.333
-56.000
-70.667
-85.333
-100.000

Fig. 10 Transverse residual stress distribution for welding (a) without and (b) and (c) with a Cu interlayer. Overall cross-section distribution of transverse residual stress for welding (d) without and (e) with a Cu interlayer.

Fig. 11(a) shows the LRS distribution curves along L_1 and L_2. The peak value of the LRS increases in the weld on both the steel and Nb sides after the addition of the Cu interlayer. The steel side increases by approximately 25 MPa, and the Nb side by nearly 50 MPa. Fig. 11(b) shows the LRS distribution curves along L_0 and l_0. By comparing the two curves, it can be seen that the longitudinal residual tensile stress at the weld also increases after the addition of the Cu interlayer. In addition, the peak residual compressive stress in the steel side increases by approximately 20 MPa in the area near 20 mm away from the weld, and the RS tends to have the same distribution as the distance increases. The residual tensile stress in the area within 20 mm away from the weld on the Nb side also increases, with a maximum increase of approximately 50 MPa. The RS in the area beyond 20 mm is basically unchanged.

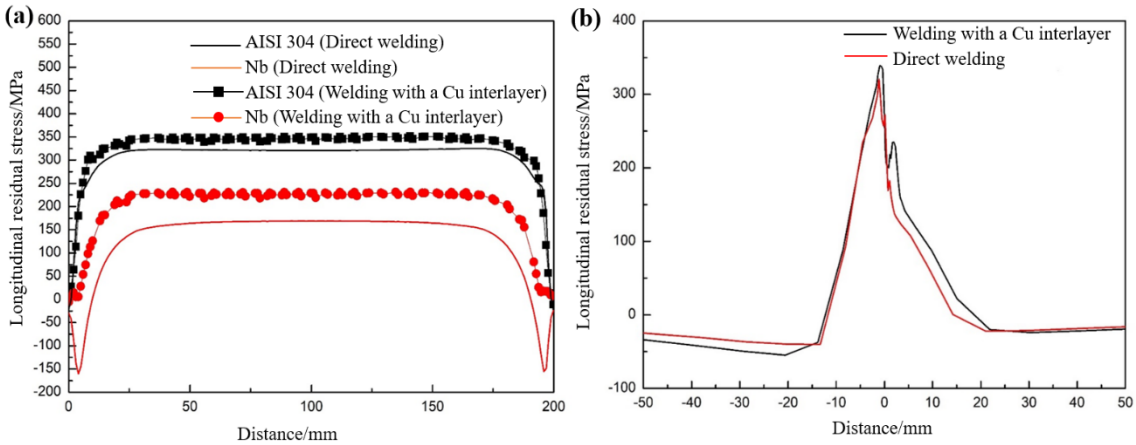

Fig. 11 Longitudinal residual stress curve (a) along the weld and (b) perpendicular to the weld.

Fig. 12 shows the transverse residual stress (TRS) distribution curves along L_1 and L_2 (Fig. 3(a)) and l_1 and l_2 (Fig. 3(b)). The comparison shows that the transverse stress on both the steel and Nb sides also increases in the direction along the weld after the

addition of the Cu interlayer. The steel side increases approximately 50 MPa, and the Nb side increases approximately 20 MPa. In addition, the distribution of RS is more complicated after the addition of the Cu interlayer because the weld consists of three different materials. Further, Cu causes a larger residual tensile stress in the welded joints, which increases by approximately 15 MPa at the fusion line and by approximately 10 MPa on the Nb side. The RS has its maximum increase at the position 10 mm away from the weld on the steel side, with an increase of 20 MPa.

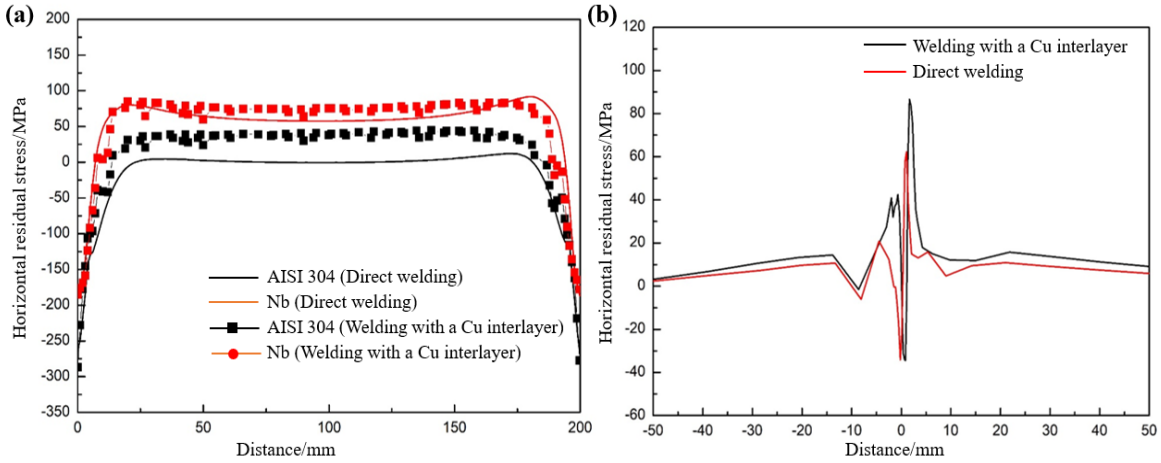

Fig. 12 Transverse residual stress curve
(a) along the weld and (b) perpendicular to the weld.

In summary, the addition of a Cu interlayer leads to an increase in RS, whether parallel or perpendicular to the weld. The reason is that the laser acted only once in direct laser offset welding, whereas double-pass laser welding is adopted when Cu is added. Under the action of two lasers, the increase in melted metal at the welded joints lead to an increase in metal shrinkage during the cooling process, which results in an increase in the RS at the joints. The strengthening mechanism of welded joints are mainly solid-solution strengthening of Cu by Fe and second-phase strengthening of Cu by Nb (Ref. 10), which indicates that the properties of welded joints are mainly determined by metallurgical factors, followed by the stress state of the joints.

5 Deformation analysis

When the joints were cooled to room temperature, the RS led to deformation. Fig. 13 shows the deformation when cooled to room temperature. The deformation on both sides of the weld in Fig. 13(a) is nearly symmetrically distributed, while in Fig. 13(b), after adding the Cu interlayer, the deformation on both sides of the weld is completely asymmetrically distributed, and more importantly, the deformation is greatly reduced. Figs. 13(c) and (d) show the angular deformation before and after the addition of a Cu interlayer. Transverse shrinkage is not uniformly distributed in the thickness direction, resulting in angular deformation. The most important deformation during direct offset welding is angular deformation, which is greatly reduced after adding the Cu interlayer.

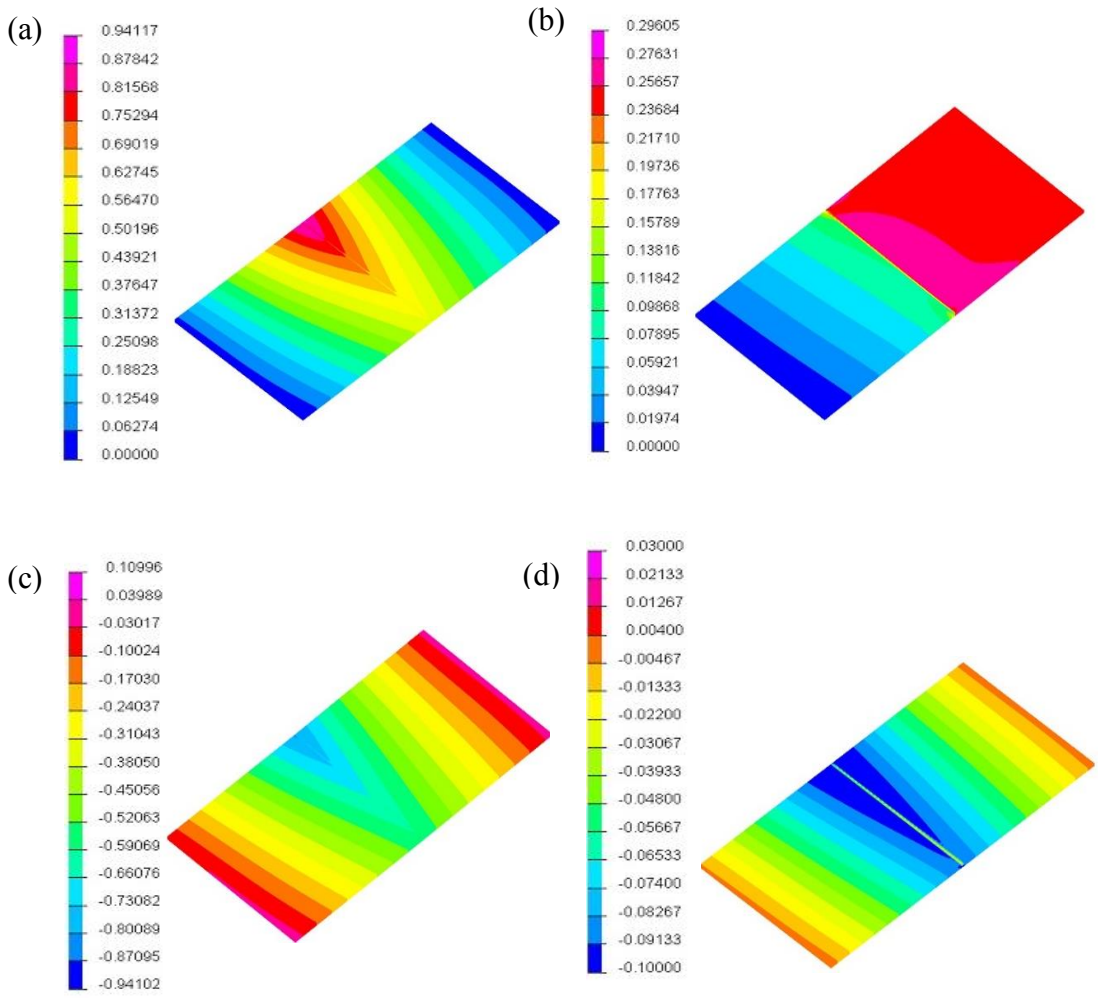

Fig. 13 Deformation image for welding (a) without and (b) with a Cu interlayer. Angular deformation image for welding (c) without and (d) with a Cu interlayer.

Fig. 14 shows the distribution curve of the angular deformation in the centre of the weld, which more intuitively reflects the reduction in angular deformation after adding the Cu interlayer. According to the cross-sectional appearance of the welded joints (Fig. 4), the shape of the molten pool of direct welding is wider at the top, while due to the high thermal conductivity of Cu, the melting of the upper and lower surfaces of the molten pool is almost the same, which leads to a smaller angular deformation.

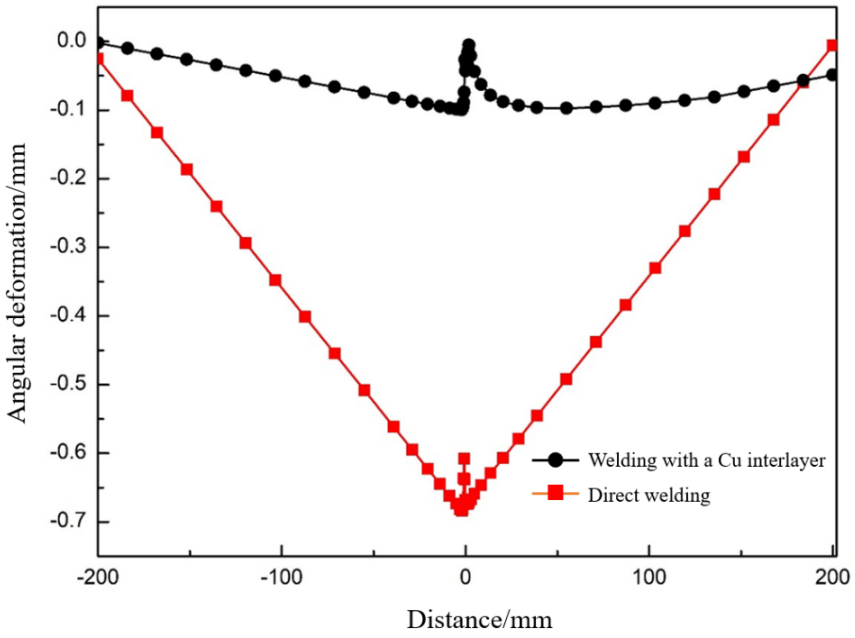

Fig. 14 Distribution curve of the angular deformation in the centre of the weld

To some extent, RS and residual deformation can affect the bearing capacity and service life of the welded structure, but for a welded joint, the influence of metallurgical factors dominates. The residual stresses state of the joints are secondary. Adding a Cu interlayer contributes to a higher RS. But Cu is a soft metal, and so the stress can be partially relieved after welding for a long time via the plastic deformation of Cu. It is conducive to improve the service life of the whole structure.

6 Conclusions

In this study, based on the completion of steel-Nb dissimilar metal laser welding, numerical simulations of the temperature field, RS field, and deformation both without and with a Cu interlayer were completed using a SYSWELD software. The effect of the addition of the Cu interlayer was analysed. The results are as follows.

(1) The temperature field distribution of both welding methods are asymmetric about the weld. The steel side heats up faster than the Nb side, and the temperature of the Nb side is higher than that of the steel side at the same distance. In addition, the addition of a Cu interlayer effectively reduces the peak temperature at the centre of the weld and decreases the temperature gradient perpendicular to the weld.

(2) After the addition of the Cu interlayer, the overall distribution trend of the residual stress does not change significantly, but both the transverse and longitudinal residual stresses increase to a certain degree. The peak values of the LRS distribution curves along L_1 and the TRS distribution curves along L_2 increase by approximately 25 MPa and 50 MPa on the steel side and nearly 50 MPa and 20 MPa on the Nb side.

(3) For the deformation, the addition of a Cu interlayer significantly reduces the weld deformation, while the uniform distribution of transverse shrinkage in the thickness direction reduces the angular deformation with a Cu interlayer.

References

[1] P. Singh, D. Deepak, G.S. Brar, Comparative evaluation of aluminum and stainless steel dissimilar welded joints, Mater. Today Proc., 2020, 2: 682–690.

[2] W. Chuaiphan, L. Srijaroenpramon, Evaluation of microstructure, mechanical properties and pitting corrosion in dissimilar of alternative low cost stainless steel grade 204Cu and 304 by GTA welding joint, J. Mater. Res. Technol., 2020, 23: 3745–3753.

[3] X. Gao, H. Liu, J. Liu, et, Laser welding of Ti6Al4V to Cu using a niobium interlayer, J. Mater. Process. Technol., 2019, 270: 293–305.

[4] A. Kumar, P. Ganesh, R. Kaul, P. Chinna Rao, D.P. Yadav, B.K. Sindal, R.K. Gupta, R.S. Sridhar, C. Joshi, and B. Singh, Process Development for Vacuum Brazed Niobium–316L Stainless Steel Transition Joints for Superconducting Cavities, J. Man. Sci. Eng., 2017, 139: 1–8.

[5] S.H. Baghjari, F.M. Ghaini, H. R. Shahverdi, C. Mapelli, S. Barella, and D. Ripamonti, Laser Welding of Niobium to 410 Steel with a Nickel Interlayer Produced by Electro Spark Deposition, Mater. Des., 2016, 107: 108–116.

[6] Y. Taran, A.M. Balagurov, B. Sabirov, V. Davydov, and A.M. Venter, Neutron Diffraction Investigation of Residual Stresses Induced in Niobium-Steel Bilayer Pipe Manufactured by Explosive Welding, Mater. Sci. Forum, 2014, 768: 697–704.

[7] J.P. Wu, Y.L. Yang, H.Z. Zhao, Q. Lin, B. Zhao, D.Z. Guo, and H.B. Su, Microstructure Analysis of the Explosive Cladding Interface of Nb/ 304L, Rare Met. Mater. Eng., 2008, 37: 634–637.

[8] X. Li, J.P. Zheng, and J. Zhao, Characteristics of Welding-Brazed Joint Between Nb-1Zr Alloy and 304 Stainless Steel, Trans. China Weld. Inst., 2011, 32: 105–108.

[9] J.C. Wang, Development and expectation of laser welding technology, Laser Technol., 2001, 25(1): 48–54.

[10] M.X Shi, Y.J Li, X. Ma, Cu Interlayer-Induced High-Strength Laser-Welded AISI 304 Steel-Niobium Joint, J. Mater. Eng. Perform., 2019; 28(9): 5369–5375.

[11] K. Saito, K. Sugiyama, K. Hiraga, Al13M4-type structures and atomic models of their twins, Mater. Sci. Eng., 2000, 294–296: 279–282.

[12] D. Travessa, M. Ferrante, G. den, Diffusion bonding of aluminium oxide to stainless steel using stress relief interlayers, Mater. Sci. Eng., 2002. 337(2): 287–296.